Image-guided Simulation of Heterogeneous Tissue Deformation For Augmented Reality during Hepatic Surgery

Nazim Haouchine, Jérémie Dequidt, Igor Peterlik, Erwan Kerrien, Marie-Odile Berger, Stéphane Cotin

Image-guided Simulation of Heterogeneous Tissue Deformation for Augmented Reality During Hepatic Surgery

Nazim Haouchine*
Inria - Shacra Team
Inria - Magrit Team

Jeremie Dequidt
Inria - Shacra Team
University of Lille

Igor Peterlik
IHU Strasbourg

Erwan Kerrien
Inria - Magrit Team

Marie-Odile Berger
Inria - Magrit Team

Stephane Cotin†
Inria - Shacra Team

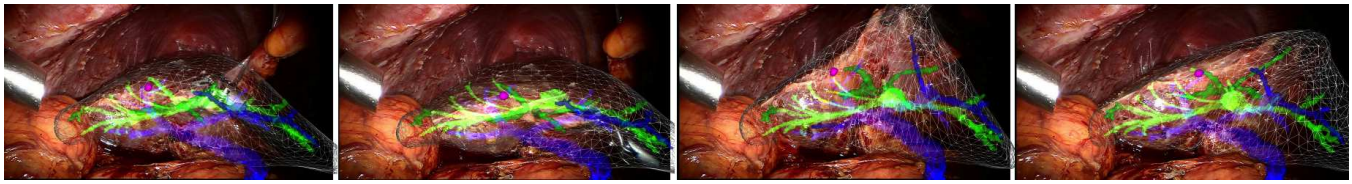

Figure 1: A sequence of images showing the superimposition of the 3D real-time biomechanical model onto the human liver, undergoing deformation due to instrument interaction during minimally invasive hepatic surgery. The liver is represented in wireframe, the tumor in purple, the hepatic vein is shown in blue and the portal vein in green.

ABSTRACT

This paper presents a method for real-time augmentation of vascular network and tumors during minimally invasive liver surgery. Internal structures computed from pre-operative CT scans can be overlaid onto the laparoscopic view for surgery guidance. Compared to state-of-the-art methods, our method uses a real-time biomechanical model to compute a volumetric displacement field from partial three-dimensional liver surface motion. This permits to properly handle the motion of internal structures even in the case of anisotropic or heterogeneous tissues, as it is the case for the liver and many anatomical structures. Real-time augmentation results are presented on *in vivo* and phantom data and illustrate the benefits of such an approach for minimally invasive surgery.

Index Terms: H.5.1 [Information Interfaces and Presentation]: Multimedia Information Systems—Artificial, augmented, and virtual realities; I.3.5 [Computer Graphics]: Computational Geometry and Object Modeling—Physically based modeling

1 INTRODUCTION

In the last decades, considerable advances in medicine have seen the emergence of Minimally Invasive Surgery (MIS). In this procedure, surgical instruments and an endoscopic camera are inserted into the abdominal cavity through small incisions in contrast of open surgery where the incisions may be large. The surgeon manipulates these instruments by watching the video stream acquired from the endoscopic camera. Although open surgery is still very common, many procedures are now performed with minimally invasive techniques considering their advantages for patient in reducing pain and time recovery. From a surgical skill standpoint these procedures are quite complex mainly because the visual feedback is relatively incomplete or poor and due to the the loss of direct organ manipulation. With recent Augmented Reality techniques, those issues can be circumvented. Internal structures computed from pre-operative scans such as tumors and vessels can be superimposed onto the intra-operative images in order to guide the surgeons during the procedure. Our study focuses on minimally invasive hepatic surgery.

In order to establish a full augmented reality system for MIS a number of difficult problems have to be solved [24]. The abdominal cavity undergoing laparoscopic surgery remains a very challenging environment for computer vision tasks. The surgical instruments interacting with the liver may cause large occlusions, the illumination variations caused by the endoscopic light and the liver bleeding or smokes due to electrocautery may disturb organ motion tracking and 3D structures recovery. Among the most difficult and still unsolved issues is the capacity to tackle, in real time, elastic deformations of the liver. The liver can undergo large deformations due to surgical tools interaction or due to respiratory motion and heart beating. Currently, most existing AR systems handle rigid motions of organs and only a very limited number of papers address the problem of elastic organ deformation.

This paper proposes an augmented reality framework that is able to estimate, in real-time, the position relevant of internal structures of the liver (vessels and tumors) taking into account liver deformations and tissue heterogeneity. The main contributions of the paper are: a) the use of an accurate biomechanical model of liver deformation accounting for heterogeneity and anisotropy due to veins and arteries; b) a real-time implementation of this virtual liver model; c) the definition of appropriate boundary conditions and external force that guide the biomechanical model using partial 3D motion estimated at the liver surface from a stereo video stream; d) the computation of the non-uniform deformation field throughout the whole volume; and e) the estimation of the position of internal structures from this volumetric displacement field. The physical model is also used as regulizer for the unreliable measurement of the visual tracking and as motion compensation in poorly textured area.

The following of the paper is organized as follows. Section 2 presents the previous works related to non-rigid registration and augmented reality in MIS. Section 3, 4 and 5 explains our approach while section 6 details the experimental results obtained on computer generated data, phantom data and *in vivo* data.

*e-mail: nazim.haouchine@inria.fr
†e-mail: stephane.cotin@inria.fr

2 Related Work

In this section we present previous works related to augmented reality for Minimally Invasive Surgery. Since we propose to address the issue of elastic liver behaviour, we first present an overview of non-rigid registration methods in AR systems. Second, previous works on AR techniques for surgery guidance are presented. In the last part, we highlight our contribution.

2.1 Non-rigid registration for AR

Non-rigid surfaces augmentation has been a topic of interest of many researchers. The need to obtain realistic augmentation both in terms of geometric behaviour and in rendering has increased the number of papers in this area. Depending on the context, non-rigid registration and augmentation can be realized directly from 2D images [22] or may take advantage of a 3D model of the shape. When the texture information on the object is rich enough, many points can be matched between images, allowing a 2D deformation motion model to be computed. Bartoli *et al.* [3] used a direct method to register non-rigid pairs of images. In their approach, Radial Basis Mapping is used as an equivalent to the optical flow constraint regularization approach [22]. In contrast to direct methods Pilet *et al.* [26] proposed a fast and robust tracking for handling large deformations. This approach uses a set of wide baseline feature matches and combines 2D deformable meshes with a robust estimation technique. Zhu *et al.* [41] proposed an approach to reduce the number of iterations of the previous method by using a progressive Finite Newton algorithm and an efficient factorization method to solve the optimization problem. In his approach Gay-Belille *et al.* [11] considered the occluded pixels as self-occlusion area that forces the wrap to shrink instead of outliers. Inspired by this self-occlusion shrinking method, Hilsmann *et al.* [15] proposed an approach exploiting an optical flow constraint regularization by a 2D deformable mesh. The advantage of such methods is that they can be applied with monocular images but they require that rich information texture is available. Another restriction is that augmentation can only be realized onto the surface of the object. Thus AR medical applications where virtual objects may be added in depth can not be handled by such techniques. To cope with this problem, 3D deformable model have been considered. The deformation can be guided by monocular images [30] [32] or directly by 3D features available on the surface acquired with stereoscopic or depth camera as in [14]. Recently, a combination of Finite Element Modelling with and Extended Kalman Filter shows the efficiency of physics-based method to recover deformations from images [1]. One of the difficulty of these approaches is to define an appropriate deformation model. Most of the time, it is computed from a representative sample of possible shapes using a dimensionality reduction process.

2.2 Augmented Reality in MIS

A number of research groups have investigated the use of AR during MIS but most contributions are dedicated to rigid organs or assume that elastic deformations between pre-operative and intra-operative data are negligible. In practice, large elastic deformations may occur due to breathing or due to the interaction of the organ with the surgeon's tools. Past attempts to perform AR on deformable organs made use of markers or navigation aids placed close to the area of navigation targets [37] or require interaction to refine elastic registration between pre and intro-operative data [24]. Others [9] build pre-operatively a dynamic 4D model of the heart which is registered to intra-operative data thanks to the use of ECG. In [36], Su *et al.* proposed and 3D-3D iterative closest point (ICP) registration with an image-based tracking to superimpose the 3D model onto laparoscopic images for kidney partial resection. Since the kidney do not actually undergo elastic deformations during surgery the 3D-3D registration is performed in a rigid manner.These methods have shown the feasibility of automatic AR systems in surgery but put constraints on the operating room, required interaction or are dedicated to specific - i.e cyclic- deformations.

Recently, significant advances have been realized towards automatic registration between pre and intra-operative data in MIS. In the context of laparoscopy and with monocular images, Kim *et al.* [17] proposed a robust solution to track and augment a deformable surgical site using shape from shading and conformal mapping. However their method only retrieves surface deformation and cannot ensure an accurate augmentation of inner structures. When augmentation with in-depth structures is required, elastic registration of the surface of the organ is no more sufficient and volume tracking has to be considered.

Mechanical-based deformable models have proven to be relevant for volume deformation tracking since they allow to define elastic properties of the shape and thus to infer in-depth motion from boundary constraints. Most of the time, simple models based on linear elasticity have been considered [31, 33, 34]. In [27], a 4D scan of the heart is coupled with a biomechanical model. It is controlled by surface constraints created by features extracted from a stereovision stream and allows quite accurate overlay of internal structures. This approach is however limited to cyclic movements where no large deformations nor surgeon manipulation occur. In [34], intra-operative registration between stereo endoscopic images and pre-operative modeling of the liver based on biomechanical properties is proposed. A linear and a Neo-hookean elastic model are considered and the accuracy of registation is assessed on a phantom. Results are slighly better with the second model but the model is not suitable for real time simulation.

A combination of physics-based model and image-based tracking was proposed in [13, 12] for vascular network augmentation during hepatic surgery. This approach used a physical model as regularization step to avoid false tracking measurement and to compute global volumic deformation despite poor image-features detection. However results are shown for very limited range of deformation, mainly when the deformation is perpendicular to camera optical axis and only visual assessment is shown.

2.3 Our contribution

We investigate here a real time deformable biomechanical approach based on a co-rotational mechanical model, provably adapted to the liver [25]. We improve upon [34] by proposing a method that does not demand a computationally expensive dense stereo surface reconstruction and integrate a measure of the quality of the 3D point reconstruction within the expression of the external forces. A preliminary version of this work was published in [12]. The contributions of the paper are:

- Introducing a real-time physics-based model to propagate in-depth surface liver motion.
- Real-time achievement using a biomechanical model taking into account tissue anisotropy and non homogeneous behaviour of the liver.
- Providing an experimental protocol to validate the accuracy of the approach. We show that the error between the estimated and actual positions of an artificial tumor implanted in a phantom liver is less than 5 mm.
- Perform in vivo tests on human data during hepatic surgery that show the capability of the tracking algorithm (since stiffness of the phantom liver and texture strongly differ from that of human liver).

The computational flow of the method is described in Figure 2.

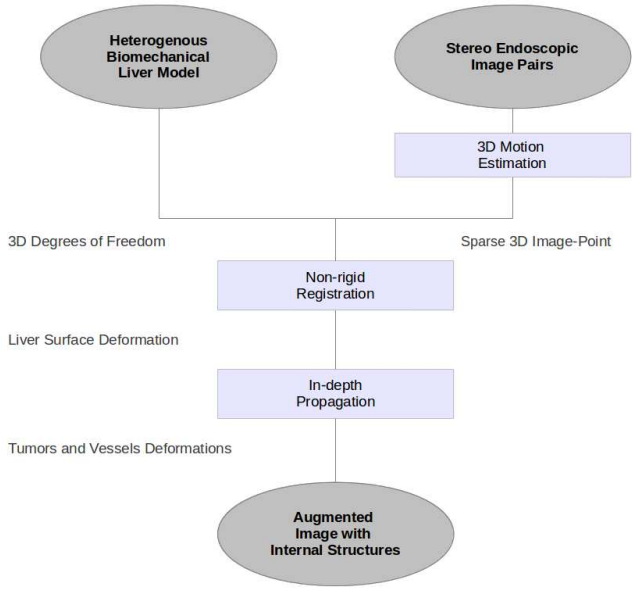

Figure 2: Computational flow of the method

3 3D Motion Estimation

Many methods have attempted to recover 3D information on the organ from intra-abdominal images [21, 27, 17, 35, 29]. In this study, a stereo endoscope is used in order to recover 3D information on the liver. Since our method only requires a set of sparse 3D points, we use feature-based tracking algorithm. Salient landmarks are detected in each image pair using the Speeded-Up Robust Features (SURF) descriptor [4] and are tracked over time thanks to the Lucas-Kanade optical flow [18]. This combination has proven to be robust to track heart motion in laparoscopic images [6]. Feature correspondences between stereo images are obtained with a nearest neighbour criterion on feature descriptors coupled with the epipolar constraint to filter out outliers. After triangulation, we obtain a sparse set of m 3D points, denoted by $3 \times m$ coordinate vector $\mathbf{y}$. Examples of point correspondences and reconstructed 3D points from laparoscopic images are shown in Fig. 3.

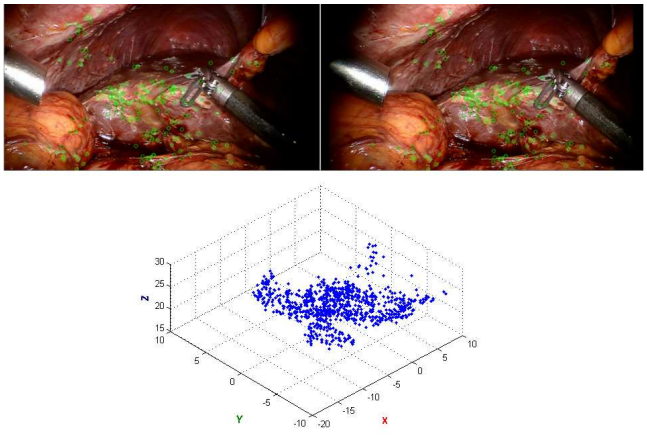

Figure 3: 3D Estimation on a laparoscopic image of the abdominal cavity showing a part of the liver. Top: SURF features detection on image pairs acquired from the Da Vinci Robot. Bottom: the resulting sparse 3D point set $\mathbf{y}$ plotted.

The SURF detector provides a measure of reliability for each extracted feature as the determinant of the Hessian matrix. We take advantage of this measure to associate each reconstructed 3D point with a quality q defined as the average reliability of its two corresponding features in the left and right images. Quality values are normalized so that $q = 1$ for the most reliable 3D point and $q = 0$ for the least reliable 3D point in $\mathbf{y}$ point set. We denote $\mathbf{q}$ the $3 \times m$ vector formed by all q values, assuming the quality is isotropic at each point. Note that other measures of reliability could be considered, such as euclidean distances of the matched descriptors or the eigenvalues of the covariance matrix on the reconstructed points.

We used two sorts of stereo endoscope, the first one consists of two mounted endoscope from Karl Storz Endoscopy and the second one is the stereo endoscope from the Da Vinci robot illustrated in 4. Both camera lens generate radial distortion and have relative small baselines (respectively 16mm and 6mm). The cameras are calibrated following Zhang [40] approach and lens distortions are rectified before performing the tracking. We take the assumption that the stereo endoscope is fixed, which is the case when the surgeon manipulate the surgical instruments.

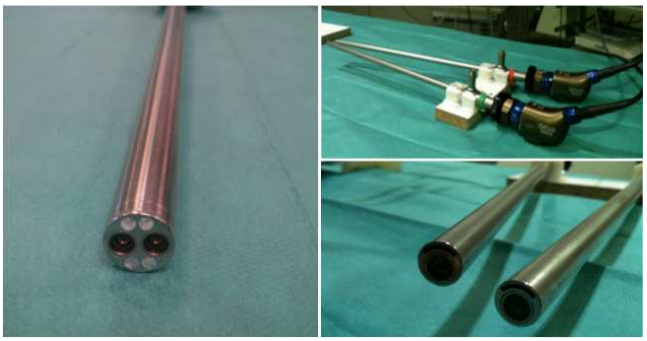

Figure 4: Stereo endoscope used: on (left) a stereo endoscope of the Da Vinci robot and (right) different views of the two mounted endoscope from Karl Storz Endoscopy.

4 Biomechanical Model

In this section we provide a description of the biomechanical model used to compute the deformations of the liver. Before giving details of tetrahedral model employed for parenchyma, we focus on model of vascularization and mechanical coupling between this two. Since the final composite model is heterogeneous and anisotropic due to the vascular structures, we finally describe the solution process based on a direct solver, still allowing for real-time performance.

4.1 Parenchyma Model

Most biomechanical studies concerning the constitutive models of the liver parenchyma (see [16] or [10] for instance) report the nonlinear and viscoelastic behavior of the organ tissue. Since we do not focus on the transient part of the deformation but rather the static equilibrium under some specific loading conditions, we do not take into account the viscous properties of the tissue. On the other hand, we aim at modeling large deformations correctly, since during the surgical interventions, important displacements of tissue (e.g. the liver lobes) occur due to the action of surgical tools.

For this reason we have opted for a finite element method based on a co-rotational formulation (introduced by Felippa in [8]) which allows for large displacements while relying on a linear expression of the stress-strain relationship. The co-rotational approach is based on decomposition of the actual element configuration into rotational and deformational components, both being quantified w. r. t. the initial position. More precisely, the actual position of the element

nodes determines the base of the element (given by three chosen adjacent edges), which is both rotated and deformed w. r. t. the initial base of the same element. In order to extract the rotational component (denoted as $\mathbf{R}_e$), a matrix decomposition such as polar, SVD or QR is needed; in our method we employ the technique described in [23]. The matrix $\mathbf{R_e}$ is used to update the local stiffness matrix $\mathbf{K_e}$ of the element. Therefore, via this element-wise rotations, the actual global stiffness matrix $\mathbf{K}$ depends in each step on the actual deformation $\mathbf{u}$ and the equation relating the external forces to the displacements can be written as

$$\mathbf{f} = \mathbf{K}(\mathbf{u})\mathbf{u} \text{ with } \mathbf{u} = \mathbf{x} - \mathbf{x}^0 \tag{1}$$

where $\mathbf{x}_0$ and $\mathbf{x}$ represent nodal positions in rest and actual positions, respectively, and $\mathbf{f}$ are the external forces.

Assuming that linear tetrahedral P1 elements are employed in the finite element formulation of the parenchyma model and the mesh is composed of $N_{\mathbb{P}}$ nodes, the resulting system has $3N_{\mathbb{P}}$ degrees of freedom, i. e. $\mathbf{u}_{\mathbb{P}}$, $_{\mathbb{P}}$ are vectors of size $3N_{\mathbb{P}}$ whereas $\mathbf{K}_{\mathbb{P}}$ is a $3N_{\mathbb{P}} \times 3N_{\mathbb{P}}$ matrix, where the subscript $\mathbb{P}$ denotes the parenchyma.

It should be noted that our method is not limited to the co-rotational model, which can be replaced by hyperelastic formulation such as the technique based on *multiplicative Jacobian energy decomposition* presented in [20].

4.2 Vessel model

The vascular system is regarded as the main source of heterogeneity which has a global influence on the mechanical response of the vascularized tissue due to important stiffness of the vessel wall. The model employed here is based on work presented in [25]. Besides describing the model in the actual scenario, additional details concerning the assembling of the composite system are given in the following text. Is should be emphasized that a potential viscoelastic response due to fluids (i. e. blood) circulating in the vessels is not taken into account as only a quasi-static scenario is assumed.

From the mechanical point of view, the vascular system is modeled with serially linked beam elements in a similar way as proposed by Duriez *et al.* [5] for simulating catheters and guide wires. This model shares some similarities with the co-rotational model described above, and in particular allows for geometrically nonlinear deformations. At the same time it accounts for rotational degrees of freedom, i. e. besides linear positions and forces, orientation and torques are included in the mechanical formulation.

We introduce some modifications to the model to take into account the particular nature of vessels, in particular through specific cross section profiles and moments of inertia (see [28] for details). The static formulation for the deformation of a beam is described by a system similar to Eq. 1 with constituents $\mathbf{u}_{\mathbb{V}}$, $\mathbf{f}_{\mathbb{V}}$ and $\mathbf{K}_{\mathbb{V}}$. However, as each node is equipped with 6 degrees of freedom due to the rotational components, the size of vectors $\mathbf{u}_{\mathbb{V}}$ and $\mathbf{f}_{\mathbb{V}}$ is $6N_{\mathbb{V}}$ and $\mathbf{K}_{\mathbb{V}}$ is a $6N_{\mathbb{V}} \times 6N_{\mathbb{V}}$ matrix where $N_{\mathbb{V}}$ is the size of beam mesh representing the geometry of vessels.

4.3 Coupling between vessel and parenchyma

In order to build the composite model of vascularized tissue, we adopt the method proposed in [25]. At the beginning of the time step, the forces applied in the beam points are propagated to the vertices of tetrahedra. Then, stiffness matrices for both beam and tetrehedral models are assembled and combined together as described below. The composite system is solved resulting in displacements of the tetrahedral vertices. Finally, the positions of beam nodes are updated based on actual positions of tetrahedra. For the sake of simplicity, we first describe the positional mapping between the nodes, then the propagation of forces and finally we show how the stiffness matrices are combined together to get the global stiffness matrix of the composite system.

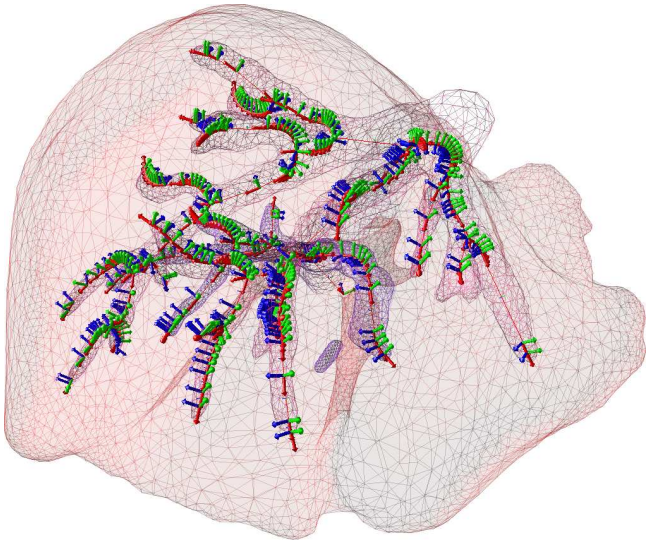

Figure 5: 3D heterogeneous biomechanical model of the liver: the rigid beam nodes representing the centerlines of vessels depicted with frames. Two vascular trees are shown: portal and hepatic veins.

Let us first focus on positional mapping of an arbitrary beam point of the vessel network. We recall that the point is defined by its position $\mathbf{p}$ and orientation $\mathbf{O}$ in space. Before the simulation starts, the point is associated with a tetrahedron T so that it is located inside T. Two quantities are precomputed for the point: the barycentric coordinates of $\mathbf{p}$ w. r. t. the tetrahedron T (denoted as β_T) and orientation $\mathbf{O}_T$ of the point formulated relatively with respect to the tetrahedron T, computed as $\mathbf{O}_T = \mathbf{B}_T^{-1}\mathbf{O}$ where $\mathbf{B}_T$ is an orthogonal base given by the edges connecting the nodes of the tetrahedron T in the rest position. It should be noted that the same matrix is required by the co-rotational model. Since it is supposed that no relative motion between the parenchyma and vessels occurs, both β_T and $\mathbf{O}_T$ remains constant during the simulation and in each step they are used to calculate the updated position $\mathbf{p}$ and orientation $\mathbf{O}$ of the beam point in space. As for the position, the calculation using the barycentric coordinates is straightforward. The updated orientation $\mathbf{O}'$ is computed as $\mathbf{O}' = \mathbf{B}'_T\mathbf{O}_T$ where $\mathbf{B}'_T$ is the base given by update positions of the tetrahedron T. The calculation of the updated base $\mathbf{B}'_T$ requires the orthogonalization process, however, this computation is already needed by the co-rotation model, so the mapping does not introduce an additional significant computational cost.

In the same time step, the response forces applied in the beam node are mapped onto the vertices of the associated tetrahedron T. For the beam point, there are linear forces $\mathbf{f}$ as well as torques τ, whereas for the tetrahedron, only linear forces $\mathbf{F}$ are modeled in the element vertices. The linear response force $\mathbf{f}$ is mapped from the beam point to its corresponding tetrahedron T using the barycentric coordinates β_T introduced above. The torques τ are transformed to the linear forces acting in the tetrahedron nodes using the equation $\tau = \mathbf{r} \times \mathbf{F}$ where $\mathbf{r}$ is vector connecting the beam and tetrahedron nodes. Putting it together, the force contribution of the beam point is added to the forces applied in the vertices of associated tetrahedron T as $\mathbf{F}_i = \mathbf{F}_i + \beta_i\mathbf{f} - (\mathbf{r}_i \times \tau)$ where i runs over the vertices of T.

As introduced above, the vascularized tissue is a composite deformable object, where the total stiffness matrix $\mathbf{K}$ is composed of contributions provided by stiffness of parenchyma $\mathbf{K}_{\mathbb{P}}$ and stiffness of vessels walls $\mathbf{K}_{\mathbb{V}}$. Let us suppose that the mapping between the beam and tetrahedra nodes can be be expressed in a matrix form

as $\mathbf{f}_{\mathbb{P}} = \mathbf{J}^T \mathbf{f}_v i$ where $\mathbf{J}$ is a $3N_{\mathbb{P}} \times 6N_{\mathbb{V}}$ Jacobian matrix of the mapping between the nodes of parenchyma and vessels [7]. The global stiffness $\mathbf{K}$ matrix is then computed as $\mathbf{K} = \mathbf{K}_{\mathbb{P}} + \mathbf{J}^\top \mathbf{K}_{\mathbb{V}} \mathbf{J}$.

Concerning the tumor, since this work focus only on small tumors, we assume that its influence on the overall mechanical behaviour is negligeable and therefore the coupling with the parenchyma is only geometric. However the tumor can easily be modelled as a real mechanical model with different properties from those of the parenchyma, which will not affect the performance of our method.

4.4 Numerical Solution

In this paper, a quasi-static scenario is considered, i. e. the actual shape of deformable object under applied forces is computed using the finite element formulation without dealing with the dynamic properties of the tissue. Therefore, in each step of the simulation, a linear system given by Eq. 1 is resolved. A wide range of direct and iterative solvers has been proposed in the past to solve such a system of equations emerging in the physics-based modeling of deformable bodies. In case of homogeneous systems in which the finite element formulation results in well-conditioned matrices, iterative solvers such as conjugate gradients have proven to be efficient techniques converging rapidly to the optimal solution. However, in our case, the final matrix $\mathbf{K}$ gathers mechanical contributions of both the parenchyma and vessel walls. As the experiments reports a significant difference in stiffness of these two components (e. g. see [38]), the composite system results in poorly conditioned matrix. In this case the convergence of iterative solvers becomes an important issue.

For this reason, we rely on direct LDL solver which requires an explicit factorization of the system matrix. Although the solver imposes more strict limitations on the size of the system being resolved, it still provides a stable real-time solution applicable to the problems considered in the scope of this paper.

5 Non-rigid Registration

5.1 Initial registration

A correct initial registration is an important step in the framework since it can significantly impact the estimated position of the tumor. For that purpose, special care must be taken during the initialization phase. Similar to related works [36], our initialisation is done manually through a Graphical User Interface following these steps:

- the real camera parameters acquired from camera calibration are loaded on the virtual camera.
- the 3D model of the liver is manually aligned on the first pair of laparoscopic images based on salient geometrical landmarks such as liver contours or surrounded ligaments (the first pair is chosen so that a large part of the liver is visible).
- the biomechanical model (including the vessels and the tumour) is deformed to better fit the laparoscopic stereo images and the 3D reconstructed point cloud.
- the boundary conditions are set by fixing the correct degrees of freedom of the biomechanical model.
- the set of three-dimensional points reconstructed using this initial stereoscopic pair of images are projected onto the liver model surface. This is done using a ray casting method, followed by a computation of barycentric coordinates describing the position of these points with respect to adjacent degrees of freedom of the biomechanical model.

In addition to providing a visual consistency, the initialization helps to define the external forces linking the degrees of freedom of the model and the 3D features extracted from the stereoscopic images. Only features that intersect the liver surface after ray-casting are kept, the features that do not belong to the liver are filtered out from laparoscopic images.

5.2 Non-rigid Registration

The non-rigid registration can be seen as an optimization problem between the three dimensional features recovered from laparoscopic images representing the liver and the biomechanical model derived from preoperative CT data. In this paper we propose to perform this registration as an error-minimization problem that accounts for the internal energy of the biomechanical E_i and the tracking energy E_t. Deriving this energy shows that an extremum (minimum) is reached when the internal forces equal the tracking forces. Thus, the internal forces are expressed as:

$$\mathbf{f_i}(\mathbf{x}) = \mathbf{R_e}\mathbf{K} \cdot (\mathbf{R_e}^\top \mathbf{x} - \mathbf{x^0}) \tag{2}$$

where $\mathbf{K}$ represents the stiffness matrix, $\mathbf{R_e}$ the co-rotational matrix and $\mathbf{x}, \mathbf{x^0}$ are vectors of size $3n$ representing the position of the n degrees of freedom of the mechanical model, respectively at any time t and time $t = 0$.

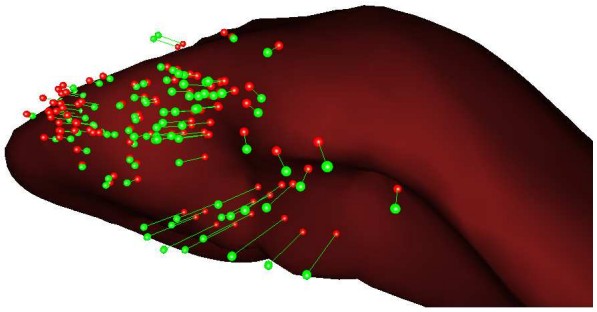

Figure 6: Non-rigid registration: one frame of the non-rigid registration where red spheres represent the projected features $\mathbf{y^0}$ from the initialisation step, green spheres represent the tracked features $\mathbf{y}$ and green lines represent the forces linking both point sets.

We propose to handle the non-rigid registration by adding external stretching forces induced by the tracking step. The tracked 3D features $\mathbf{y}$ represent how visible parts of the liver are moving. Due to noise or other reconstruction inaccuracies, point locations in $\mathbf{y}$ are often regularized by generating a smooth and dense surface model that is later used as boundary conditions for the biomechanical model [34]. Instead, we propose here to incorporate such inaccuracies directly in the mechanical solver using quality values measured at each 3D point.

External forces are defined by pairing the m 3D points $\mathbf{y}$ to the n degrees of freedom $\mathbf{x}$ of the bio-mechanical model. As explained in 5.1, the tracked points $\mathbf{y^0}$ at initialization ($t = 0$) are expressed in barycentric coordinates of the adjacent degrees of freedom leading to the linear relation:

$$\mathbf{y^0} = \mathbf{L} \cdot \mathbf{x^0} \tag{3}$$

where $\mathbf{L}$ is a rectangular $(3m, 3n)$ matrix. We assume this linear relation remains valid during the deformation. At any later time t, the stretching forces induced by the tracking are defined as

$$\mathbf{f_t}(\mathbf{y}) = k \cdot \mathbf{q} \cdot (\mathbf{y} - \mathbf{y^0}) \tag{4}$$

where k can be seen as a stiffness. Finally, the stretching forces can be expressed with respect of the degrees of freedom as

$$\mathbf{f_t}(\mathbf{x}) = \mathbf{L}^\top \cdot \mathbf{f_t}(\mathbf{y}) = \mathbf{f_t}(\mathbf{x}) = \mathbf{L}^\top \cdot k \cdot \mathbf{q} \cdot \mathbf{L} \cdot (\mathbf{x} - \mathbf{x^0}) \tag{5}$$

Parameter k is set to be one or two order of magnitude higher than the Youngs modulus in order to impose the boundary conditions directly and to insure that the simulation remains stable even at large integration steps.

6 Validation and Results

In laparoscopic surgery, validation remains very challenging. In our case, this problem is more complex since neither qualitative results nor visual assessment can validate the deformation of internal structures that are not visible in laparoscopic images. In order to asses the performance of our approach, we compared our simulation results against three experimental scenarios. First, we demonstrate with computer-generated data whether and where an heterogeneous model differs from an homogeneous one for the prediction of tumor location. Second, we rely on a realistic phantom liver to quantitatively measure the error between the simulation and a ground truth. Third, our approach is tested on an actual laparoscopic procedure performed on a human liver, allowing us to qualitatively estimate how our approach could perform in a real surgical environment.

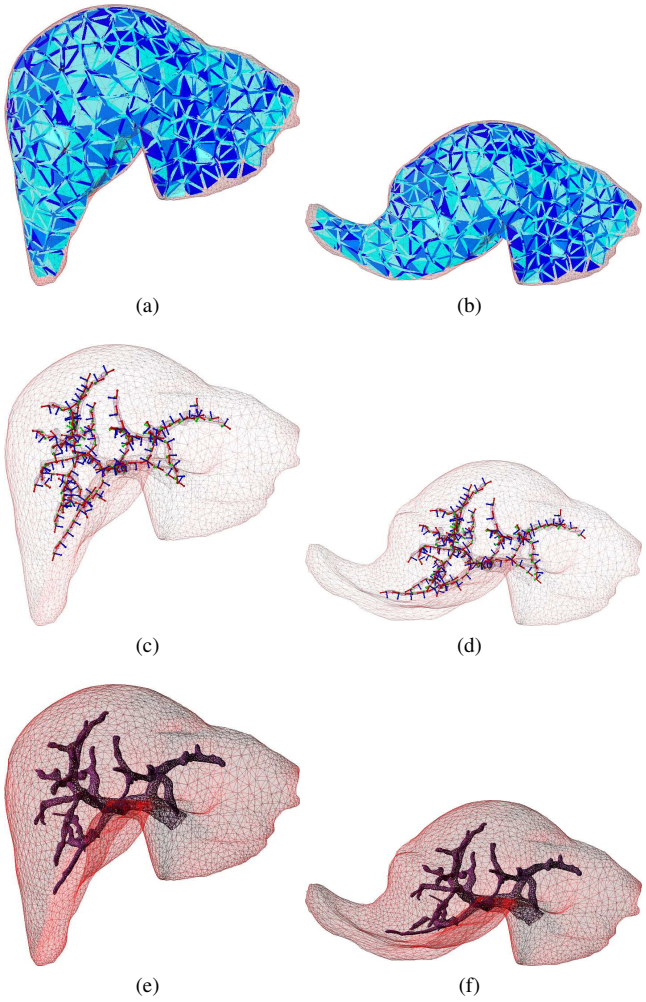

Figure 7: Computer-generated data with (left) the liver at rest and (right) the liver after deformation: in (a) and (b) the volumetric mesh composed of tetrahedra, in (c) and (d) the beams generated along the vessels described in Section 4 an in (e) and (f) the heterogenous liver including the vascular network in wireframe.

6.1 Experimentation with computer-generated data

We evaluate the impact, on the registration, of using a heterogeneous model instead of a homogeneous model (which can be seen as providing similar results as an advanced geometric approach). This is done by calculating the euclidean distance between the estimated tumor location in the cases of homogeneous and heterogeneous deformations (see 7). We also measure this influence depending on the location of the tumor in the liver, at three different locations: 1) close to the the point of interaction in order to quantify local deformation, 2) away from the point of interaction to quantify global behaviour, and 3) in the middle of the vascular network to assess its influence. The simulations are generated using the SOFA framework [2].

Results illustrated in figure 8 show that taking into account the vascular network impact the tumor location. We can notice a difference in distance of about 15 mm in the case where the tumor is located close to the deformation. We also notice that even if the tumor is located far from the point of interaction, it remains influenced by the vascular network with a distance of more than 3 mm. However, when the tumor is very close to the boundary conditions, the impact of the vascular network is considerably reduced, which is an expected result.

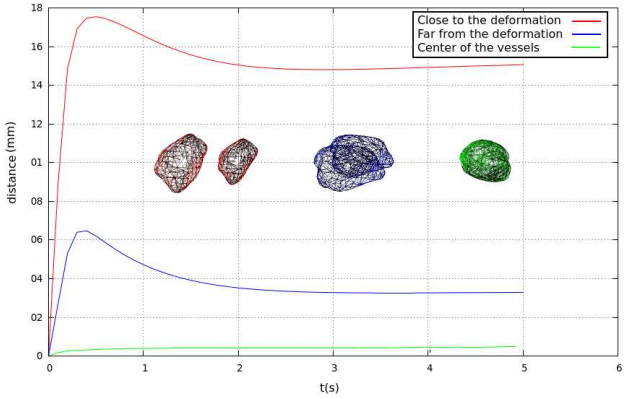

Figure 8: Impact of the vascular network on the tumor deformation depending on its position in the liver: the distance between the tumor using homogeneous and heterogeneous biomechanical model is important locally (red) and globally (blue) and less important when the tumor is constrained by the vessels. The meshes illustrate the distance between the position of the tumor in a homogeneous and a heterogeneous case for each location in the liver.

6.2 Experimentation with liver phantom data

We believe that performing a CT scan of the a phantom liver before and after a deformation is an ideal way of defining a ground truth for the location of an internal structure (e.g. a tumor). However, surgical instruments as well as the laparoscopic camera produce large image artifacts in an *in vivo* environment. Also, boundary conditions on the liver are difficult to identify while they largely influence the organ motion and deformation. Therefore we designed a validation protocol using a heterogeneous phantom liver with a prior knowledge of its mechanical properties and geometry. The geometry of the liver and vascular network is generated from an actual patient liver (but with a 1:2 scale). The laparoscopic camera is placed outside the scanned area and the deformation is created using a wire attached to the phantom to enable artifact-free CT acquisitions.

The scenario involved the following steps (described in figure 9): 1) perform a CT scan of the phantom at rest (first scan); 2) place laparoscopic camera; 3) pull on wire attached to the liver to induce

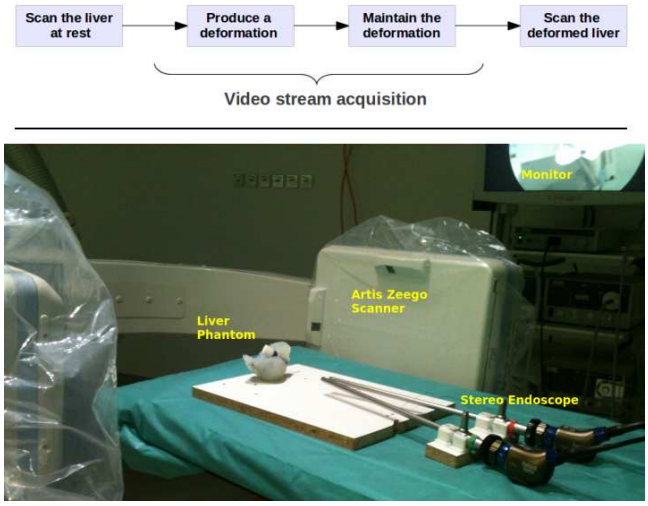

Figure 9: Experimental protocol for the quantitative validation: (top) the validation protocol and (bottom) an overview of the setup including the phantom liver, a stereoscopic camera and a partial view of the Artis Zeego imaging system. The wire hooked to the lobe is pulled and maintained in position while performing a new CT scan to provide a ground truth deformation.

a deformation of one lobe of the liver while laparoscopic images are being recorded; 4) attach the wire to freeze the deformation; 5) perform a CT scan of the deformed liver (second scan). The protocol setup is illustrated in Figure 9.

The phantom liver is a heterogeneous phantom including a vascular network and two tumors. The phantom is made of silicone with Young's Modulus E=0.15 MPa and Poisson's ratio ν=0.45 and manually textured with salient marks to perform the tracking. The video stream is acquired in 25 FPS by the two mounted endoscopes (Karl Storz Endoscopy) with a resolution of 720×576 pixels (described in Section 3). According to [6] the parameters of the Lucas-Kanade optical flow consist of a window size of 51×51 pixels and an interframe motion threshold of 20 pixels. The scans are performed with the Siemens Artis Zeego Scanner which produce high quality dynamic CT scans. A result of the three-dimensional reconstruction form CT scans is illustrated in figure 10.

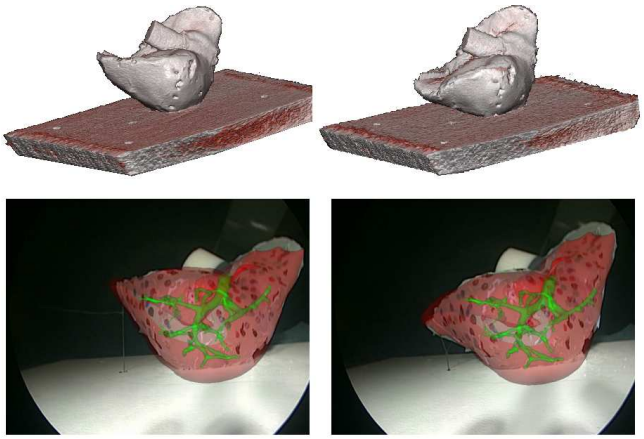

Figure 10: CT-scans: [Top] 3D reconstructed phantom at rest (left) and after deformation (right), [bottom] the registered 3D model including the vessels, at rest (left) and after deformation (right).

Using the reconstructed data from the CT acquisitions (segmented using ITK-Snap[1]), we have measured the following data using our method:

- For the first tumor: the displacement due to the deformation was 15.14 mm. At the end of the simulation, the measured distance between the centers of mass of the simulated and actual tumors was **4.40 mm**.
- For the second tumor: the displacement due to the deformation was 11.92 mm. At the end of the simulation, the measured distance between the centers of mass of the simulated and actual tumors was **3.41 mm**.

It represents a significant improvement over current laparoscopic procedures since a safety margin up to 25 mm around the possible location of the tumor (estimated from pre-operative CT-scan) is usually considered [19].

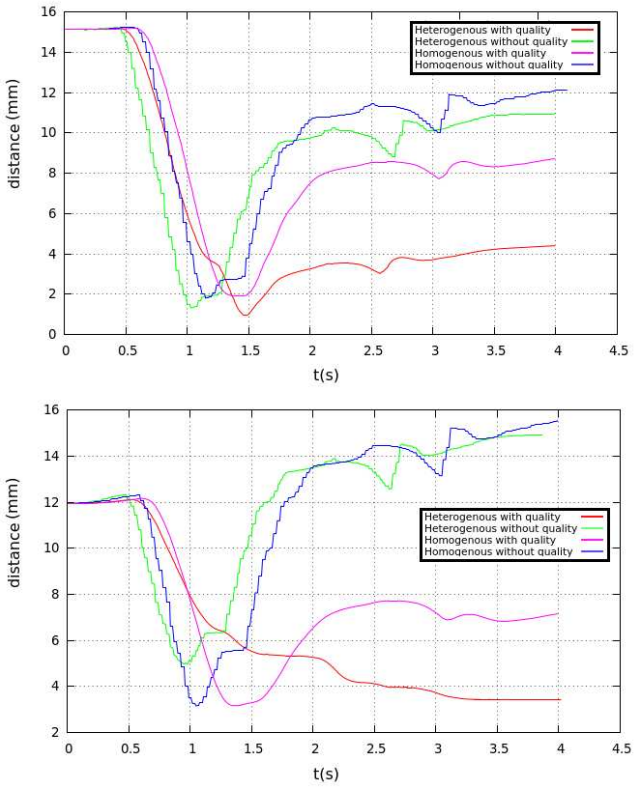

Figure 11: A comparison study between homogeneous and heterogeneous models, taking into account the feature quality. The introduction of the feature quality as well as the use of a heterogeneous model reduce considerably the error between the predicted tumor and the scanned one. We may also notice that at t=1s, the error is the smallest. This can be explained by the fact that the predicted tumor get close to the scanned one and moves away due to the low stiffness of the liver. This low stiffness is compensated while coupling the parenchyma with a stiffer vascular networks in the heterogeneous cases.

To assess the need of a heterogeneous biomechanical model, a comparison with a homogeneous model is conducted (cf figure 11). This comparison also includes the impact of the introduction of the feature quality in computing external forces. The results show that the use of a heterogeneous model reduces considerably the distance

[1] http://www.itksnap.org

between the scanned tumor at rest and the estimated one, about 4.2 mm for the first tumor and 2.5 mm for the second tumor depending of the location of the tumors. The feature quality impact on this distance is also considerable, about 6.5 mm for the first tumor and 10 mm for the second tumor

It is worth mentioning the comparison is done with the same data and parameters, and using the same estimation of the initial registration. As a consequence, the only source of difference between the results is the computation of the internal and external forces.

6.3 Results on *in vivo* human liver

When dealing with an actual patient, quantitative validation implies major technical challenges as well as ethical issues. Our approach was conducted on a laparoscopic sequence taken during a real examination. Our aim was to assess the robustness of the tracking in a real environment (specular lights, beating heart, respiratory motion, instrument occlusions, and difference between porcine and human liver textures) and the performance of our non-rigid registration. In addition, since the texture of the phantom and the wide baseline of the two mounted endoscopes may bias the tracking robustness, *in vivo* experimentations are needed.

We used elastic parameters according to [39, 38, 25]: Young's modulus of parenchyma $E_{\mathbb{P}}$=27 KPa and Poisson's ratio $\nu_{\mathbb{P}}$=0.45, Young's modulus of vessel wall: $E_{\mathbb{V}}$=0.62 MPa and Poisson's ratio $\nu_{\mathbb{V}}$=0.45, thickness of the vessel wall: $t_{\mathbb{V}}$=200 μm. The models was composed of 3391 linear P1 tetrahedral elements (parenchyma) and 120 beam elements (vasculature). The simulation employing this model was running stably in real-time: refresh rate of 25 FPS was achieved on PC having Intel i7 M620 2.76GHz processor with 960×540 images acquired from the Da Vinci Robot from Intuitive Surgical. It showed a qualitatively good liver surface and internal structures motion and deformation. Figure 12 displays 4 frames of the augmentation computed during the simulation and Figure 13 illustrated some cases when the approach may fail.

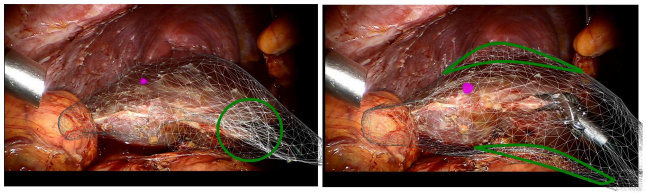

Figure 13: Failed cases: external stretching forces with high stiffness may unbalance the minimization equation and forces the model to fit the tracked points that may be poorly estimated. Bad registered areas are surrounded by green.

7 Conclusion

This work addresses several important limitations that currently hinder the use of augmented reality in the clinical routine of minimally invasive procedures. We particularly focus on the three-dimensional localization and visualization of internal structures, such as blood vessels and tumors. To this end, we have developed an image-guided biomechanical model that is able to capture the complex deformations underwent by the liver during surgery. The deformation model is guided by both internal forces (associated to a biomechanically validated model of the liver) and external forces related to three-dimensional points (reconstructed from stereo images) which incorporate a quality measure of their reliability. Such characteristics make our model able to capture both the organ surface and inner structures motion while being parameterized with textbook Young's modulus and Poisson's ratio values. Promising results were obtained through *in vivo* qualitative assessment on a human liver and quantitative validation on a phantom liver where errors well below the current surgical margins were measured. More validation is obviously required though it is worth mentioning that validation implying actual organs are seldom reported in previous works. A quantitative evaluation of the impact of the initial registration on the tumor position has to be conducted, and several cases have to be studied in order to more assess the method. The correct visualization of the tumor and the vessels (in terms of textures, shaders and lightening) was not addressed in our work and represents one of our future works. Our current method is able to cope with occluded or newly tracked points. Future work will address its robustness against actual clinical conditions where smoke, bleeding, or other surgical events may hinder the tracking.

Acknowledgements

The authors wish to thank Fernand Martel, Mario Sanz Lopez, Mourad Bouhadjar and Gael Fouré for helping us with the validation setup and data acquisition process.

References

[1] A. Agudo, B. Calvo, and J. M. M. Montiel. Finite element based sequential bayesian non-rigid structure from motion. In *CVPR*, pages 1418–1425, 2012.

[2] J. Allard, S. Cotin, F. Faure, P. J. Bensoussan, F. Poyer, C. Duriez, H. Delingette, and L. G. B. Sofa - an open source framework for medical simulation. In *Medicine Meets Virtual Reality (MMVR 15)*, 2007.

[3] A. Bartoli and A. Zisserman. Direct estimation of non-rigid registration. In *In British Machine Vision Conference*, 2004.

[4] H. Bay, A. Ess, T. Tuytelaars, and L. Van Gool. Speeded-up robust features (SURF). *Comput. Vis. Image Underst.*, 110(3):346–359, June 2008.

[5] C. Duriez, S. Cotin, J. Lenoir, and P. Neumann. New approaches to catheter navigation for interventional radiology simulation. *Computer Aided Surgery*, 2006.

[6] H. Elhawary and A. Popovic. Robust feature tracking on the beating heart for a robotic-guided endoscope. *Int J Med Robot.*, pages 459–468, Oct. 2010.

[7] F. Faure, C. Duriez, H. Delingette, J. Allard, B. Gilles, S. Marchesseau, H. Talbot, H. Courtecuisse, G. Bousquet, I. Peterlik, and S. Cotin. SOFA: A Multi-Model Framework for Interactive Physical Simulation. In Y. Payan, editor, *Soft Tissue Biomechanical Modeling for Computer Assisted Surgery*. Springer, June 2012.

[8] C. Felippa and B. Haugen. A unified formulation of small-strain corotational finite elements: I. theory. *Computer Methods in Applied Mechanics and Engineering*, 194(21):2285–2335, 2005.

[9] M. Figl, D. Rueckert, D. Hawkes, R. Casula, M. Hu, O. Pedro, D. P. Zhang, G. Penney, F. Bello, and P. Edwards. Image guidance for robotic minimally invasive coronary artery bypass. *Computerized Medical Imaging and Graphics*, 34(1):61–68, 2010.

[10] Z. Gao, T. Kim, D. L. James, and J. P. Desai. Semi-automated soft-tissue acquisition and modeling forsurgical simulation. In *Proceedings of the fifth annual IEEE international conference on Automation science and engineering*, CASE'09, pages 268–273, Piscataway, NJ, USA, 2009. IEEE Press.

[11] V. Gay-Bellile, A. Bartoli, and P. Sayd. Direct estimation of nonrigid registrations with image-based self-occlusion reasoning. *IEEE Trans. Pattern Anal. Mach. Intell.*, 32(1):87–104, Jan. 2010.

[12] N. Haouchine, J. Dequidt, M.-O. Berger, and S. Cotin. Deformation-based Augmented Reality for Hepatic Surgery. In *Medicine Meets Virtual Reality, MMVR 20*, San Diego, USA, 2013.

[13] N. Haouchine, J. Dequidt, E. Kerrien, M.-O. Berger, and S. Cotin. Physics-based Augmented Reality for 3D Deformable Object. In *VRIPHYS - Virtual Reality Interaction and Physical Simulation*, Darmstadt, Germany, Dec. 2012.

[14] T. Hayashi, F. de Sorbier, and H. Saito. Texture overlay onto non-rigid surface using commodity depth camera. In *International Conference on Computer Vision Theory and Applications*, pages 66–71, 2012.

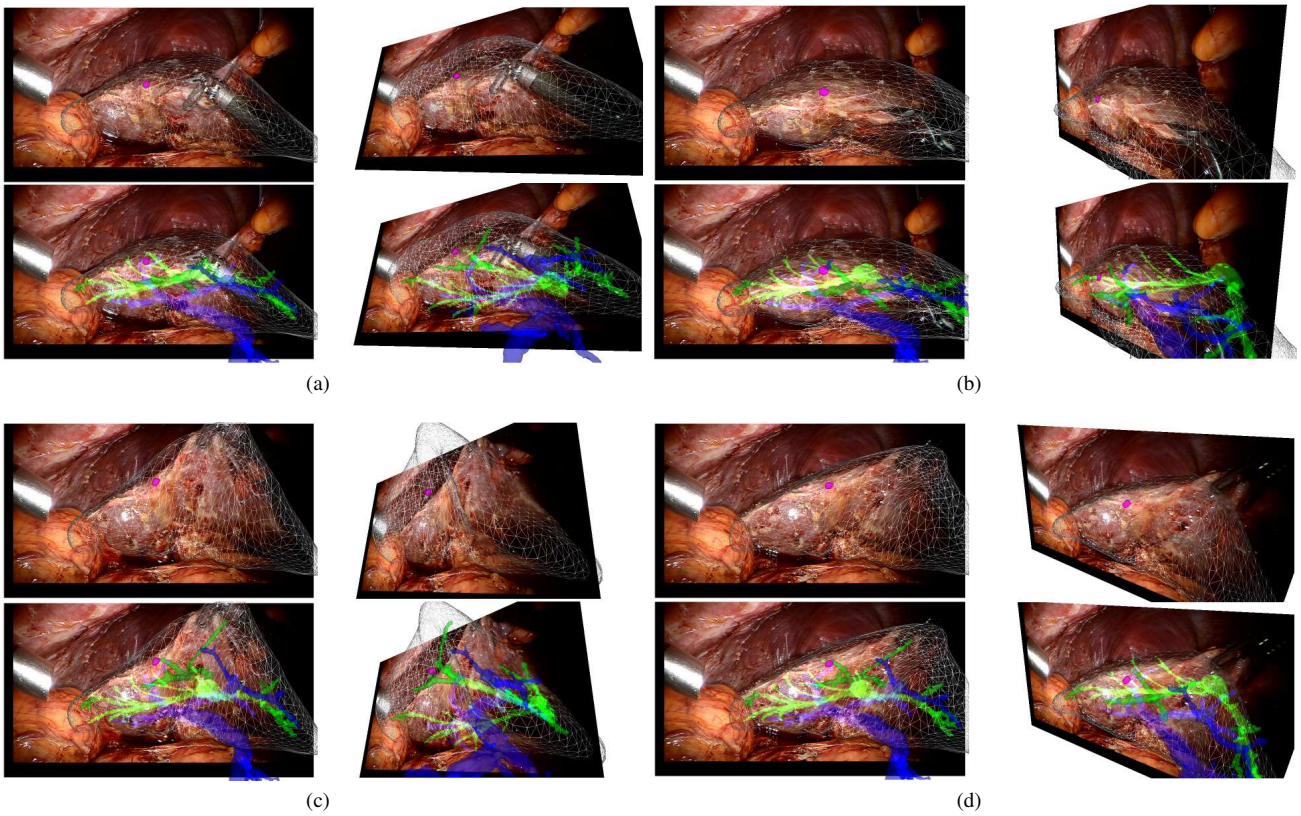

Figure 12: A sequence of images showing, in different views, the superimposition of the real-time biomechanical model onto the human liver undergoing deformation due to surgical instrument interaction during MIS. The liver is represented in wireframe, the tumor in purple, the hepatic vein is shown in blue and the portal vein in green.

[15] A. Hilsmann, D. C. Schneider, and P. Eisert. Realistic cloth augmentation in single view video under occlusions. *Comput. Graph.*, 34(5):567–574, Oct. 2010.

[16] A. E. Kerdok, M. P. Ottensmeyer, and R. D. Howe. Effects of perfusion on the viscoelastic characteristics of liver. *Journal of Biomechanics*, 39:2221–2231, 2006.

[17] J.-H. Kim, A. Bartoli, T. Collins, and R. Hartley. Tracking by detection for interactive image augmentation in laparoscopy. In *Proceedings of the 5th international conference on Biomedical Image Registration*, WBIR'12, pages 246–255. Springer-Verlag, 2012.

[18] B. D. Lucas and T. Kanade. An iterative image registration technique with an application to stereo vision. In *Proceedings of the 7th international joint conference on Artificial intelligence - Volume 2*, IJCAI'81, pages 674–679, San Francisco, CA, USA, 1981. Morgan Kaufmann Publishers Inc.

[19] T. Mala, B. Edwin, I. Gladhaug, E. Fosse, O. Sreide, A. Bergan, and O. Mathisen. A comparative study of the short-term outcome following open and laparoscopic liver resection of colorectal metastases. *Surgical Endoscopy And Other Interventional Techniques*, 16(7):1059–1063, 2002.

[20] S. Marchesseau, T. Heimann, S. Chatelin, R. Willinger, and H. Delingette. Multiplicative jacobian energy decomposition method for fast porous visco-hyperelastic soft tissue model. In *MICCAI 2010*, volume 6361 of *LNCS*, pages 235–242. 2010.

[21] X. Maurice, P. Graebling, and C. Doignon. Real-time structured light coding for adaptive patterns. *Journal of Real-Time Image Processing*, pages 1–10, 2011.

[22] A. Mitiche and P. Bouthemy. Computation and analysis of image motion: a synopsis of current problems and methods. *Int. J. Comput. Vision*, 19(1):29–55, July 1996.

[23] M. Nesme, Y. Payan, and F. Faure. Efficient, physically plausible finite elements. In J. Dingliana and F. Ganovelli, editors, *Eurographics 2005, Short papers, August, 2005*, Trinity College, Dublin, Irlande, 2005.

[24] S. Nicolau, L. Soler, D. Mutter, and J. Marescaux. Augmented reality in laparoscopic surgical oncology. *Surgical Oncology*, 20(3):189 – 201, 2011.

[25] I. Peterlík, C. Duriez, and S. Cotin. Modeling and real-time simulation of a vascularized liver tissue. In *Proceedings of the 15th international conference on Medical Image Computing and Computer-Assisted Intervention - Volume Part I*, MICCAI'12, pages 50–57. Springer-Verlag, 2012.

[26] J. Pilet, V. Lepetit, and P. Fua. Fast non-rigid surface detection, registration and realistic augmentation. *Int. J. Comput. Vision*, 76(2):109–122, Feb. 2008.

[27] P. Pratt, D. Stoyanov, M. Visentini-Scarzanella, and G.-Z. Yang. Dynamic guidance for robotic surgery using image- constrained biomechanical models. In *Proceedings of the 13th international conference on Medical image computing and computer-assisted intervention: Part I*, MICCAI'10, pages 77–85. Springer-Verlag, 2010.

[28] J. S. Przemieniecki. *Theory of Matrix Structural Analysis*. 1985. Reprint of McGraw Hill, 1968.

[29] R. Richa, A. P. L. Bó, and P. Poignet. Robust 3d visual tracking for robotic-assisted cardiac interventions. In *Proceedings of the 13th international conference on Medical image computing and computer-assisted intervention*, MICCAI2010, pages 267–274. Springer-Verlag, 2010.

[30] M. Salzmann, J. Pilet, S. Ilic, and P. Fua. Surface deformation models for nonrigid 3d shape recovery. *IEEE Trans. Pattern Anal. Mach. Intell.*, 29(8):1481–1487, Aug. 2007.

[31] M. Sermesant, C. Forest, X. Pennec, H. Delingette, and N. Ayache. Deformable biomechanical models: Application to 4D cardiac image

analysis. *Medical Image Analysis*, 7(4):475–488, 2003.

[32] S. Shen, W. Shi, and Y. Liu. Monocular 3-d tracking of inextensible deformable surfaces under l2-norm. *Trans. Img. Proc.*, 19(2):512–521, Feb. 2010.

[33] T. Shen, H. Li, and X. Huang. Active volume models for medical image segmentation. *IEEE Trans. Med. Imaging*, 30(3):774–791, 2011.

[34] S. Speidel, S. Roehl, S. Suwelack, R. Dillmann, H. Kenngott, and B. Mueller-Stich. Intraoperative surface reconstruction and biomechanical modeling for soft tissue registration. In *Proc. Joint Workshop on New Technologies for Computer/Robot Assisted Surgery*, 2011.

[35] D. Stoyanov. Stereoscopic scene flow for robotic assisted minimally invasive surgery. In *Proceedings of the 15th international conference on Medical Image Computing and Computer-Assisted Intervention*, MICCAI2012, pages 479–486. Springer-Verlag, 2012.

[36] L.-M. Su, B. P. Vagvolgyi, R. Agarwal, C. E. Reiley, R. H. Taylor, and G. D. Hager. Augmented reality during robot-assisted laparoscopic partial nephrectomy: Toward real-time 3d-ct to stereoscopic video registration. *Urology*, 73(4):896 – 900, 2009.

[37] D. Teber, S. Guven, T. Simpfendrfer, M. Baumhauer, E. O. Gven, F. Yencilek, A. S. Gzen, and J. Rassweiler. Augmented reality: A new tool to improve surgical accuracy during laparoscopic partial nephrectomy? preliminary in vitro and in vivo results. *European Urology*, 56(2):332 – 338, 2009.

[38] S. Umale, S. Chatelin, N. Bourdet, C. Deck, M. Diana, P. Dhumane, L. Soler, J. Marescaux, and R. Willinger. Experimental in vitro mechanical characterization of porcine glisson's capsule and hepatic veins. *Journal of Biomechanics*, 44(9), 2011.

[39] H. Yamada. *Strength of biological materials*. The williams and Wilkins Company, Baltimore, 1970.

[40] Z. Zhang. A flexible new technique for camera calibration. *IEEE Trans. Pattern Anal. Mach. Intell.*, 22(11):1330–1334, Nov. 2000.

[41] J. Zhu and M. R. Lyu. Progressive finite newton approach to real-time nonrigid surface detection. In *Computer Vision and Pattern Recognition, 2007. CVPR'07. IEEE Conference on*, pages 1–8. IEEE, 2007.